THE JOURNAL OF PHYSICAL CHEMISTRY Letters

Letter

Cite This: J. Phys. Chem. Lett. 2019, 10, 270−277

pubs.acs.org/JPCL

Orientational Dynamics of Transition Dipoles and Exciton Relaxation in LH2 from Ultrafast Two-Dimensional Anisotropy

Sara C. Massey,[†] Po-Chieh Ting,[†] Shu-Hao Yeh,[†,‡] Peter D. Dahlberg,[§,#] Sara H. Sohail,[†] Marco A. Allodi,[†] Elizabeth C. Martin,[∥] Sabre Kais,[⊥] C. Neil Hunter,[∥] and Gregory S. Engel*[,†]

[†]Department of Chemistry, Institute for Biophysical Dynamics, and the James Franck Institute, The University of Chicago, Chicago, Illinois 60637, United States

[‡]Qatar Environment and Energy Research Institute, Hamad Bin Khalifa University, Qatar Foundation, Doha, Qatar

[§]Graduate Program in the Biophysical Sciences, Institute for Biophysical Dynamics, and the James Franck Institute, The University of Chicago, Chicago, Illinois 60637, United States

[∥]Department of Molecular Biology and Biotechnology, University of Sheffield, Firth Court, Western Bank, Sheffield S10 2TN, United Kingdom

[⊥]Department of Chemistry, Purdue University, West Lafayette, Indiana 47907, United States

Supporting Information

ABSTRACT: Light-harvesting complexes in photosynthetic organisms display fast and efficient energy transfer dynamics, which depend critically on the electronic structure of the coupled chromophores within the complexes and their interactions with their environment. We present ultrafast anisotropy dynamics, resolved in both time and frequency, of the transmembrane light-harvesting complex LH2 from *Rhodobacter sphaeroides* in its native membrane environment using polarization-controlled two-dimensional electronic spectroscopy. Time-dependent anisotropy obtained from both experiment and modified Redfield simulation reveals an orientational preference for excited state absorption and an ultrafast equilibration within the B850 band in LH2. This ultrafast equilibration is favorable for subsequent energy transfer toward the reaction center. Our results also show a dynamic difference in excited state absorption anisotropy between the directly excited B850 population and the population that is initially excited at 800 nm, suggesting absorption from B850 states to higher-lying excited states following energy transfer from B850*. These results give insight into the ultrafast dynamics of bacterial light harvesting and the excited state energy landscape of LH2 in the native membrane environment.

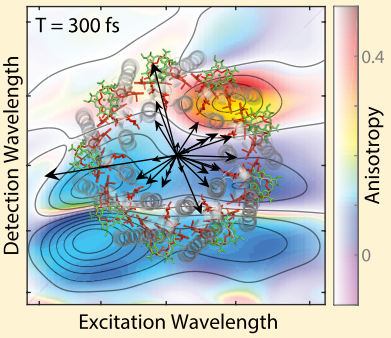

Transmembrane pigment−protein complexes harvest light from the sun and transfer energy to the reaction center (RC) with high quantum efficiency.[1] In purple bacteria, the peripheral antenna, light-harvesting complex 2 (LH2), contains 27 bacteriochlorophyll *a* (BChl *a*) arranged in two distinct rings termed B800 and B850 according to their wavelengths of maximum absorption (Figure 1a inset).[2] This dense packing of chromophores within a protein scaffold is common to light-harvesting complexes and results in a complicated electronic structure with a manifold of excitonic states. Energy migrates through LH2 from B800 to B850 on a 700−800 fs time scale[3−5] and undergoes ultrafast intra-B850 band energy transfer from higher-lying B850* excited states in 60−200 fs.[6] LH2 in *Rhodobacter sphaeroides* (*Rba. sphaeroides*) absorbs solar energy and transfers excitations to energetically downstream light-harvesting complex 1 (LH1) and then to the RC to initiate photochemistry.[1,7,8] After absorption, excitations in LH2 undergo exciton relaxation, during which their transition dipoles can reorient. This reorientation is constrained by the two-dimensional ring structure of LH2.[6,9,10] Exciton localization and the time dependence of transition dipole orientations will produce transient anisotropy, which can be readily measured with polarization-dependent experiments. Generalized Förster theory suggests that the degree of excitation delocalization within B800 and B850 influences the energy transfer and relaxation processes.[11] This delocalization has been probed by pump−probe anisotropy, photon echo peak shift, and superradiance experiments.[12−16]

Two-dimensional electronic spectroscopy (2DES)[17−19] provides information not accessible in pump−probe experiments by providing frequency resolution in both the excitation and detection domains while maintaining ultrafast time resolution. By controlling the polarization of the laser pulses, we can observe transient anisotropic dynamics of pigment−protein complexes. Anisotropy in multidimensional spectroscopy has been used to monitor the orientational dynamics of transition dipoles in hydrogen bonding networks in water both experimentally[20−22] and theoretically.[23] Recently, the approach

Received: October 22, 2018
Accepted: January 1, 2019
Published: January 1, 2019

DOI: 10.1021/acs.jpclett.8b03223
J. Phys. Chem. Lett. 2019, 10, 270−277

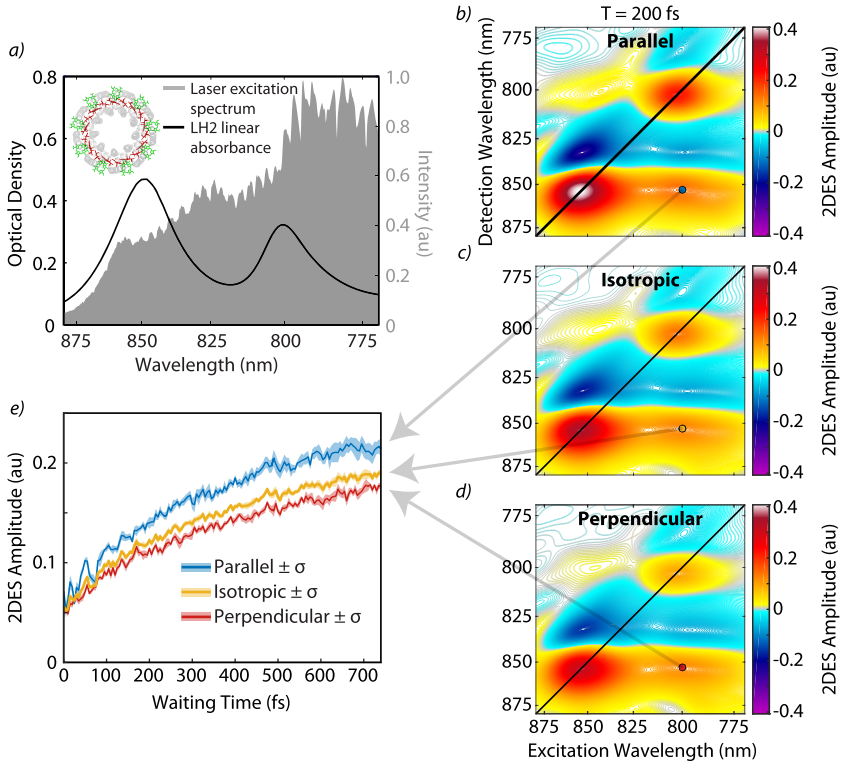

Figure 1. (a) Linear absorbance of LH2-only membranes in a 200 μm path length and the laser excitation spectrum (gray shaded area) used in two-dimensional electronic spectroscopy (2DES) experiments. The laser spectrum is broad enough to interrogate both the B800 and B850 bands. The inset shows the crystal structure of LH2 from *Rps. acidophila* (PDB ID: 1NKZ).[2] B800 and B850 rings of BChl *a* are shown in green and red, respectively, with phytyl tails removed for visual clarity. (b–d) Absorptive 2DES spectra of LH2-only membranes at a waiting time of 200 fs for (b) all-parallel $\langle ZZZZ \rangle$, (c) isotropic $\left(\frac{\| +2 \perp}{3}\right)$, and (d) perpendicular $\langle XXZZ \rangle$ polarization sequences. (e) Waiting time traces shown as an average of six scans from the SE/GSB crosspeak feature (λ_{exc} = 800 nm, λ_{det} = 853 nm) for all-parallel (blue) and perpendicular (red) experiments and the calculated isotropic (yellow) response. The shaded area indicates ± the standard error of the mean (σ) from six scans.

revealed excitonic hopping on carbon nanotube thin films,[24] enabled spectral feature assignment in chlorophylls,[25] and showed vibrational relaxation and energy transfer in an explosive.[26] Other polarization-dependent third-order spectroscopy experiments have been utilized to suppress and amplify selected pathways[27−30] and to probe changes in transition dipoles such as quantum coherences in LH2.[31]

In this Letter, we extend the application of two-dimensional anisotropy spectroscopy to study the anisotropic dynamics of LH2. We follow the dynamics of transition dipole reorientation in this light-harvesting complex to improve our understanding of the excited state energy landscape. We are able to reproduce the temporal trends in our 2D anisotropy spectra using modified Redfield theory. In 2DES, three time-ordered ultrafast pulses interact with the sample, resulting in a third-order polarization that generates a stimulated emission (SE)/ ground state bleach (GSB)/ excited state absorption (ESA) signal in a phase-matched direction. Two-dimensional spectra correlate excitation wavelengths (λ_{exc}) with detection wavelengths (λ_{det}) of SE/GSB/ESA at a given waiting time, T.[19] 2DES spectra are collected using the GRadient Assisted Photon Echo Spectroscopy (GRAPES) apparatus that spatially encodes the time delay between pulses 1 and 2, the coherence time, τ.[32] The all-parallel, $\langle ZZZZ \rangle$, and perpendicular, $\langle XXZZ \rangle$, excitation pulse sequence polarizations are acquired separately using an achromatic half-wave plate to rotate the polarization of pulses 1 and 2 by 90°.

For this anisotropy study, LH2 in its native membrane environment was prepared from an LH2-only mutant of *Rba. sphaeroides*.[33] Details of the preparation of membrane fragments can be found in the Supporting Information. The laser excitation spectrum used for 2DES experiments covered the Q_y absorbance peaks of both B800 and B850 (Figure 1a). Parallel and perpendicular 2DES spectra in Figure 1b,d reveal similar spectral features with a positive SE/GSB diagonal peak at 800 nm corresponding to B800, a strong diagonal B850 feature with contributions from SE/GSB (positive) just below the diagonal near 850 nm, and ESA (negative) just above the diagonal near 850 nm. Energy transfer from B800 to B850 corresponds to the growth of the SE/GSB and ESA crosspeaks in the lower right quadrant. These features are consistent with previous 2DES studies on isolated LH2 and live cells of *Rba. sphaeroides*.[33−35] Additional waiting time traces from the B800, B850, and lower crosspeak features are shown in Figure S1 in the Supporting Information.

To construct the Hamiltonian and simulate 2D electronic and anisotropy spectra using modified Redfield theory, we need the geometric orientation of transition dipoles and the couplings between them. A high-resolution crystal structure is not available for LH2 from *Rba. sphaeroides*. Cryoelectron microscopy of LH2 in *Rba. sphaeroides* demonstrates C_9 symmetry of its molecular aggregation.[36] Due to the lack of high-resolution crystal structures, the positions of transition dipole moments of BChls are adopted from a high-resolution crystal structure of LH2 from *Rps. acidophila* (PDB ID: 1NKZ)

DOI: 10.1021/acs.jpclett.8b03223
J. Phys. Chem. Lett. 2019, 10, 270−277

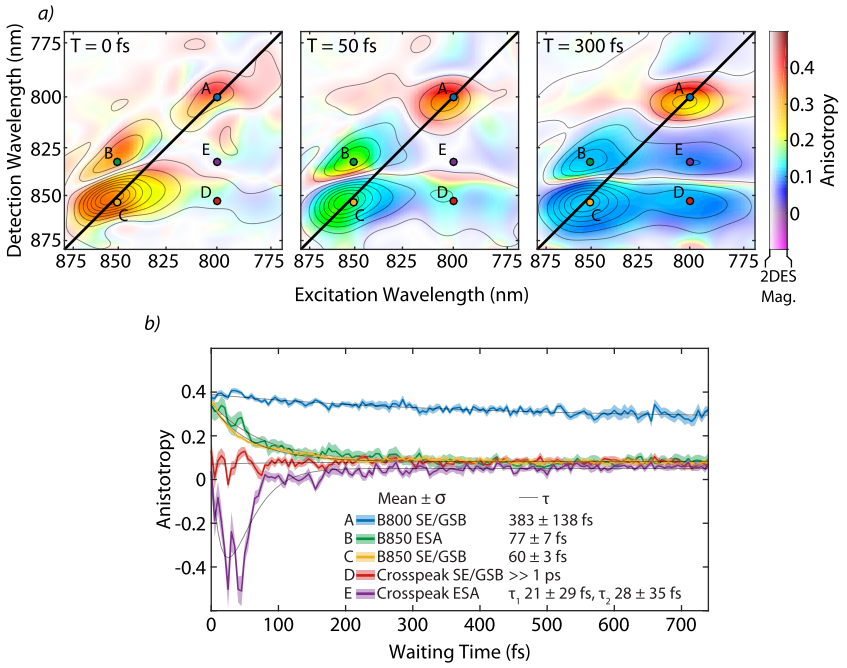

Figure 2. (a) Waiting time series of 2DES anisotropy in LH2-only membranes at 0, 50, and 300 fs. The color saturation level and gray contours indicate the all-parallel 2DES signal magnitude at the corresponding waiting time. Colored dots indicate points corresponding to the waiting time traces in (b). (b) Waiting time traces of anisotropy from the B800 diagonal SE/GSB (λ_{exc} = 800 nm, λ_{det} = 800 nm [A, blue]), B850 diagonal ESA (λ_{exc} = 850 nm, λ_{det} = 832 nm [B, green]), B850 diagonal SE/GSB (λ_{exc} = 850 nm, λ_{det} = 854 nm [C, yellow]), crosspeak SE/GSB (λ_{exc} = 800 nm, λ_{det} = 853 nm [D, red]), and crosspeak ESA (λ_{exc} = 800 nm, λ_{det} = 832 nm [E, purple]). The shaded area indicates ± standard error of the mean (σ) from six scans. The gray traces indicate the monoexponential fit to traces A–D and the biexponential fit to trace E (refer to the Supporting Information for fit details).

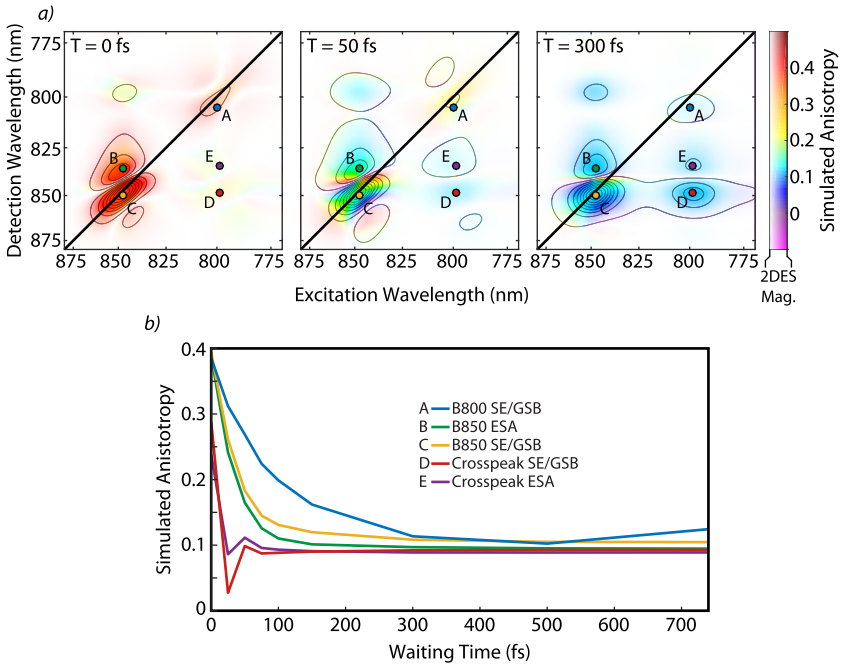

Figure 3. (a) Simulated waiting time series of 2DES anisotropy in LH2 at 0, 50, and 300 fs. The color saturation level and gray contours indicate the simulated all-parallel 2DES signal magnitude at the corresponding waiting time. Colored dots indicate points corresponding to the waiting time traces in (b). (b) Waiting time traces of simulated anisotropy from the B800 diagonal SE/GSB (λ_{exc} = 800 nm, λ_{det} = 805 nm [A, blue]), B850 diagonal ESA (λ_{exc} = 847 nm, λ_{det} = 836 nm [B, green]), B850 diagonal SE/GSB (λ_{exc} = 847 nm, λ_{det} = 850 nm [C, yellow]), crosspeak SE/GSB (λ_{exc} = 799 nm, λ_{det} = 849 nm [D, red]), and crosspeak ESA (λ_{exc} = 799 nm, λ_{det} = 834 nm [E, purple]).

with the same 9-fold symmetry, as shown in Figure 1a.[2] A previous study showed that the circular dichroism (CD) spectra of LH2 complexes from various purple bacteria primarily fall into two categories, *molischianum*-like or *acidophila*-like, and *Rba. sphaeroides* is considered to be in the former category.[37] Because CD spectroscopy is sensitive to

DOI: 10.1021/acs.jpclett.8b03223
J. Phys. Chem. Lett. 2019, 10, 270–277

the orientations of transition dipole moments, we adopted the orientations of the BChl Q_y transition dipoles from the crystal structure of LH2 from *Rsp. molischianum* (PDB ID: 1LGH[38]) and separately applied rotations on B800, B850α, and B850β transition dipole moments as in Georgakopoulou et al. to better align with the reported features in CD spectra of LH2 from *Rba. sphaeroides* and maintain a 9-fold symmetry.[37,39] Detailed information on the model parameters and all simulated 2D electronic and anisotropy spectra (Figures S2 and S3) are provided in the Supporting Information.

The time-dependent anisotropy signal $r(T)$ for each (λ_{exc}, λ_{det}) point on the 2DES spectrum was calculated by combining the parallel ($I_{\parallel}$) and perpendicular ($I_{\perp}$) absorptive time-dependent signals in the following equation

$$r(T) = \frac{I_{\parallel}(T) - I_{\perp}(T)}{I_{\parallel}(T) + 2I_{\perp}(T)} \quad (1)$$

A waiting time series of 2DES anisotropy spectra (Figure 2a) reveals correlations between the transition dipoles at the excitation wavelength and those at the detection wavelength at several waiting times. Anisotropy spectra at additional waiting times are shown in Figure S4. An alternative representation of anisotropy spectra at early waiting times is shown in Figure S5. Waiting time traces (Figure 2b) show time-dependent anisotropic dynamics from various features in the spectra. These results are reproducible over multiple experimental runs, as shown in the Supporting Information (Figures S7−S9).

The measured anisotropy of the B850 SE/GSB feature (trace C in Figure 2b) reveals a fast 60 ± 3 fs decay of the anisotropy signal, starting at 0.35 and decaying to approximately 0.1. The anisotropy of the B800 main diagonal peak (trace A in Figure 2b) starts close to 0.4 and decays on a ∼400 fs time scale. These results agree with published transient absorption anisotropy experiments.[6,10,40] The rapid anisotropy decay of the B850 SE/GSB corresponds to ultrafast reorientation of the B850 transition dipoles.[14,41] Simulated anisotropy spectra (Figure 3a) and the waiting time trace (trace C in Figure 3b) reproduce these dynamics. Novoderezhkin et al. attribute the 300−400 fs B800 anisotropy decay to one-exciton coherence dynamics;[6] however, our data do not cover sufficiently long waiting times to observe the picosecond time scale interchromophore hopping in the B800 ring.[6,10] In our simulations, the B800 anisotropy decay (trace A in Figure 3b) is faster than the experimental anisotropy decay of this feature. We are unable to definitively assign this difference, but the faster decay seen in simulation may be due to coherence dynamics, which is not included in the model.

In addition to B800 (A) and B850 (C) diagonal SE/GSB signals, we also observe the anisotropy dynamics of the B850 diagonal ESA (trace B in Figure 2b) feature, which was inaccessible in prior experiments. The B850 diagonal ESA feature (B) shows an initial anisotropy of 0.34 at T = 0 fs. An anisotropy value of 0.34 indicates preferential alignment of ESA with the initial excitation transition dipole. This result indicates that once the system has been polarized along a given axis the system is more polarizable along that axis than along any other axis. The anisotropy rapidly decays to approximately 0.1 with a 77 ± 7 fs lifetime due to ultrafast reorientation and randomization of transition dipoles on B850, similar to that observed in the diagonal B850 SE/GSB (C) feature. This result is also in agreement with simulation (trace B in Figure 3b), which shows a rapid anisotropy decay from a value of 0.42.

The crosspeak SE/GSB (trace D in Figure 2b) has an approximately constant anisotropy across the measured waiting times. This crosspeak corresponds to SE/GSB from the B850 ring following energy transfer from B800 and B850*, which occurs on respective time scales of 700−800 and 60−200 fs.[6] The anisotropy dynamics show some oscillatory structure at T < 100 fs, which may result from energy transfer from B850* to B850, but this signal is less clear than the crosspeak ESA (E) anisotropy dynamics due to overlap with strong couplings in the spectral region of the crosspeak SE/GSB (D). Energy transfer from an initially localized B800 state into the B850 ring results in an immediately random orientation of the transition dipole in the plane of the ring, indicating transfer into a delocalized B850 state, as evidenced by the constant ∼0.1 anisotropy value of the crosspeak SE/GSB (D). If the system retained memory of the initial B800 transition dipole orientation following energy transfer before reorienting, we would expect the anisotropy dynamics of the crosspeak SE/GSB (D) to resemble the anisotropy of the B850 SE/GSB (C) and ESA (B) features with an ultrafast decay from ∼0.4.

A waiting time anisotropy trace from the lower crosspeak ESA (trace E in Figure 2b) shows initial ultrafast growth of a negative anisotropy signal, followed by ultrafast decay of this negative anisotropy to approach a constant anisotropy value of ∼0.1 at T > 100 fs. This anisotropy is distinctly different from the dynamics of the lower crosspeak SE/GSB (D), which is flat across the range of waiting times, and additionally different from the B850 SE/GSB (C) and ESA (B) anisotropies, which only decay. While the B850 diagonal ESA (B) and the B850 diagonal SE/GSB (C) features show identical dynamics, the crosspeaks ESA (E) and SE/GSB (D) are fundamentally different from one another. At early waiting times (T < 50 fs), the growth of a negative anisotropy of the crosspeak ESA (E) may correspond to ESA from B850 to higher-lying excited states following energy transfer from B850*. B850* states are higher-lying states in the B850 manifold that spectrally overlap with B800 and additionally relax to B850 on the 60−200 fs time scale.[6] Calculated energies of the B850* states at different realizations of the static disorder are shown in Figure S10. This time scale of energy transfer from B850* to B850 corresponds to the ultrafast rise of the negative anisotropy signal. Dynamics corresponding to these B850* states will overlap spectrally with the B800 diagonal and crosspeak features, as opposed to the B850 diagonal features. At later waiting times, this ESA signal originating from B850* would be overwhelmed by ESA from B850 following energy transfer from B800, which supports why the negative anisotropy only persists for <100 fs.

ESA from B850 to higher-lying excited states following energy transfer from B850* may correspond to energy transfer to or from a state with out-of-plane character to give rise to an anisotropy of <0.1 at early times. In fluorescence experiments, a negative anisotropy value arises from relaxation or energy transfer to a state with the transition dipole oriented 45−135° from the initially excited state; transfer or relaxation between states with orthogonal transition dipoles yields an anisotropy value of −0.2.[42,43] Nonlinear anisotropy experiments are sensitive to differences in transition dipole orientation between different electronic states in ESA signals in addition to reporting on changes in orientation due to relaxation and energy transfer.[43] The anisotropy measurement of an ESA feature correlates the initial excitation transition dipole

DOI: 10.1021/acs.jpclett.8b03223
J. Phys. Chem. Lett. 2019, 10, 270−277

moment orientation (in this case, B850*) with the transition dipole moment orientation of the ESA transition (in this case, B850 to a higher-lying excited state). In the case of a two-dimensional ring structure, like LH2, the anisotropy could correspond to ESA to and from a state in which the transition dipole is coplanar to the ring following energy transfer from a state in which the transition dipole is orthogonal to the plane of the ring (or vice versa). The B850* transition dipoles have significant out-of-plane character and in many instances of static disorder are oriented >45° from the plane of the LH2 ring (Figure S11). Energy transfer from an out-of-plane B850* state to B850 states parallel to the plane of the ring and then subsequent ESA to higher-lying excited states parallel to the plane of the ring would be in agreement with these negative anisotropy signals. At longer times (T > 100 fs), the anisotropy of the crosspeak ESA feature is close to 0.1, indicating that the transition dipole moment orientation is randomly distributed but constrained to be coplanar to the ring.[12,14,40,44]

The B850 SE/GSB feature also shows a trend of anisotropy decay constants across the excitation wavelength axis (λ_{exc}) (Figure 4). A series of points from the same detection wavelength (854 nm) after being excited at varying wavelengths across the B850 band reveal that those excited on the blue edge show faster anisotropy decay. An excitation wavelength of 839.6 nm yields an anisotropy decay constant of 27.6 ± 2.7 fs, whereas an excitation wavelength of 862.6 nm yields an anisotropy decay constant of 72.0 ± 5.9 fs. This trend of faster anisotropy decay at bluer excitation wavelengths moving across the B850 SE/GSB band is reproduced in our simulation (Figure 5). In pump−probe anisotropy experiments, Nagarajan et al. showed a faster anisotropy decay with 827 nm excitation than that with 850 nm excitation, but they did not see a continuous trend across excitation wavelengths.[12] These higher-energy excitons relax quickly, resulting in a faster loss of transition dipole orientation and more rapid anisotropy decay than excitons on the red edge of the band. Segatta et al. calculated an increasing relaxation rate with increasing energy in LH2 B850 excitons using TD-DFT/MMPol at cryogenic temperature.[45] The rapid relaxation of higher-energy excitons in the B850 band limits back transfer to favor downstream energy transfer to LH1 and the RC. Similar directional behavior has been observed in LH1 in vivo.[46]

We have measured the first 2DES anisotropy spectra of membrane-bound LH2 from *Rba. sphaeroides*. We observed an orientational preference for ESA on the B850 ring and detected an ultrafast anisotropy decay of B850 ESA (B) that matches the magnitude and time scale of the ultrafast anisotropy decay of the previously established B850 SE/GSB (C). We also observed negative anisotropy at early waiting times in the crosspeak ESA (E), which may be due to ESA following energy transfer to B850 from B850* states that overlap spectrally with the B800 ring. Our results show ultrafast relaxation of higher-energy excitons within the B850 manifold, which is favorable for directing excitons toward the RC. These data reveal dynamics underlying the B850 2DES peak that are uniquely accessible with anisotropy experiments. These experimental results agree with our simulated 2D anisotropy spectra. We believe that this extension of anisotropy in 2DES will serve as a new paradigm of probing ultrafast orientational dynamics of transition dipoles and exciton dynamics on systems with confined geometry.

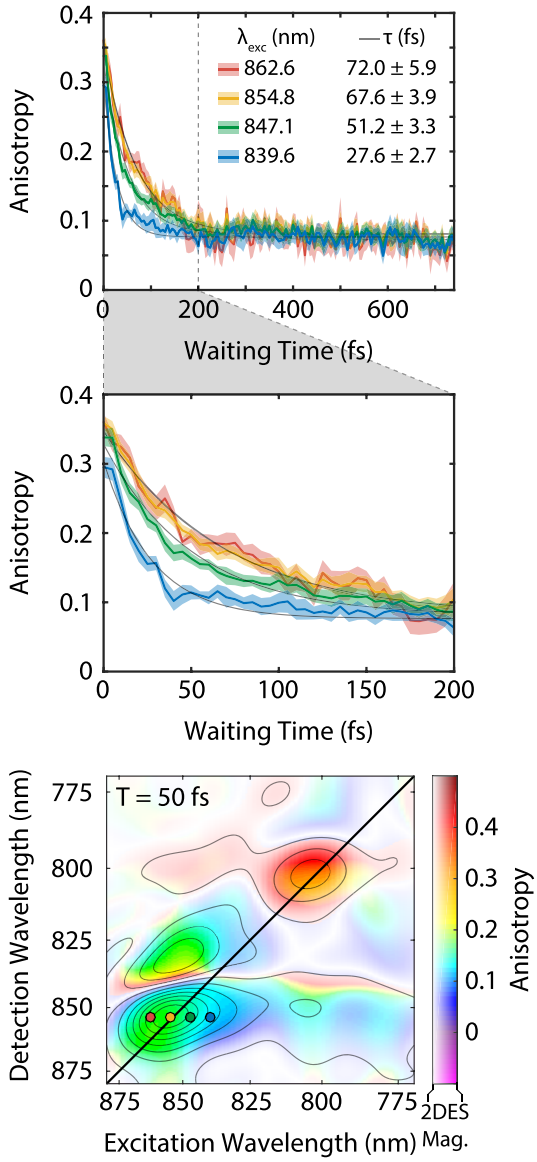

Figure 4. Waiting time traces of anisotropy from the SE/GSB B850 feature at varying λ_{exc} values and λ_{det} = 854 nm. The shaded area indicates ± the standard error of the mean (σ) from six scans. Gray traces show the monoexponential fit to each waiting time trace. The middle panel zooms in on the first 200 fs. Colored dots on the 2D anisotropy spectrum from T = 50 fs show the spectral locations of the corresponding waiting time traces.

EXPERIMENTAL METHODS

The principles and experimental setup of 2DES have been detailed elsewhere.[19] The data in this Letter were acquired using GRAPES.[32] The pulse used in this experiment was generated by a 5 kHz regenerative amplifier seeded by a Ti:sapphire oscillator (Coherent Inc.). The pulse was then passed through 2 m of argon gas (15 psi above atmospheric) and an SLM-based pulse shaper (Biophotonics Inc.) to obtain sub-25 fs pulses. Polarization rotation was achieved using a broad-band achromatic half-wave plate (Union Optic cemented, achromatic, zero order, 500−900 nm). Wave plate bandwidth performance is characterized in Figure S12. Integrated power across the beam at the time of the experiment showed suppression > 113:1. 2DES correlates absorption frequency with signal frequency as a function of a

DOI: 10.1021/acs.jpclett.8b03223
J. Phys. Chem. Lett. 2019, 10, 270−277

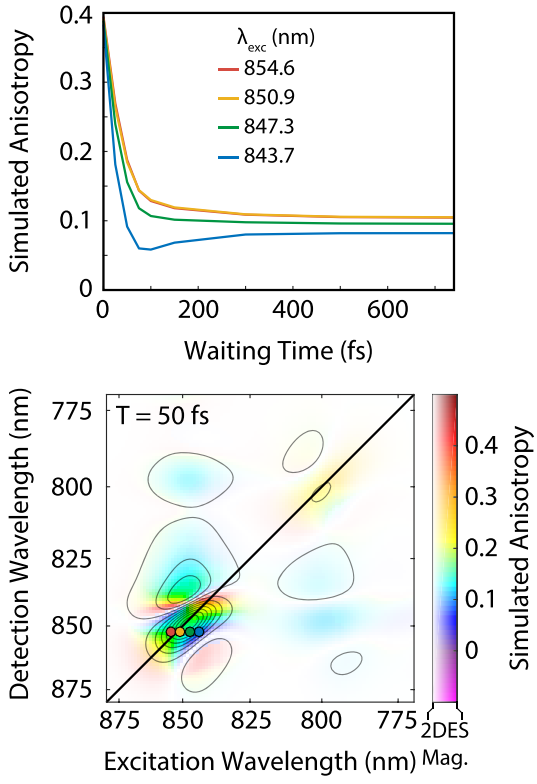

Figure 5. Simulated waiting time traces of anisotropy from the SE/GSB B850 feature at varying λ_{exc} values and λ_{det} = 852 nm. Colored dots on the simulated 2D anisotropy spectrum from T = 50 fs show the spectral locations of the corresponding waiting time traces.

time delay between pulses 2 and 3, waiting time T, which was continuously scanned by a mechanical translation stage at a speed of 1.5 μm/s. The signal was heterodyned with an attenuated local oscillator pulse and spectrally resolved with an Andor Shamrock spectrometer, followed by detection on a high-speed CMOS 2D array camera (Phantom Miro M310) at a collection rate of 50 Hz. Absorptive spectra were produced by reconstructing the nonrephasing component of the data according to Sohail et al.[46] The absolute phase of the 2D spectra was determined by fitting to separately acquired pump−probe spectra according to the projection-slice theorem.[19,34] All parallel and perpendicular 2D spectra were normalized to the global maximum of the averaged parallel spectra.

■ ASSOCIATED CONTENT

Supporting Information

The Supporting Information is available free of charge on the ACS Publications website at DOI: 10.1021/acs.jpclett.8b03223.

Sample preparation of LH2-only membranes; modified Redfield simulation parameters; additional data acquisition and processing details; mono- and biexponential fit details; 2DES waiting time traces from additional features; simulated 2DES spectra; 2DES anisotropy spectra at additional waiting times; alternative representation of 2DES anisotropy spectra; anisotropy time traces from additional spectral locations; 2DES waiting time traces, anisotropy spectra, and anisotropy time traces from an additional data set; calculated exciton energies and transition dipole orientations; and characterization of wave plate bandwidth performance (PDF)

■ AUTHOR INFORMATION

Corresponding Author

*E-mail: gsengel@uchicago.edu. Phone: 773-834-0818.

ORCID

Sara C. Massey: 0000-0002-1602-3325
Marco A. Allodi: 0000-0002-3289-1659
Sabre Kais: 0000-0003-0574-5346
C. Neil Hunter: 0000-0003-2533-9783
Gregory S. Engel: 0000-0002-6740-5243

Present Address

#P.D.D.: Department of Chemistry, Stanford University, Stanford, CA 94305.

Notes

The authors declare no competing financial interest.

■ ACKNOWLEDGMENTS

The authors thank the Vannevar Bush Faculty Fellowship program (Grant No. N00014-16-1-2513 and N00014-15-1-0048) and Air Force Office of Scientific Research (AFOSR) (Grant No. FA9550-14-1-0367 and FA9550-18-1-0099) for their support of this work. The authors acknowledge partial support from an NSF MRSEC grant (DMR-1420709). S.C.M. and S.H.S. individually acknowledge support from the Department of Defense (DoD), AFOSR, through the National Defense Science & Engineering Graduate Fellowship (NDSEG) Program, 32 CFR 168a. P.D.D. acknowledges support from the NSF-GRFP program and the National Institute of Biomedical Imaging and Bioengineering of the National Institutes of Health (T32-EB009412). M.A.A. acknowledges support from a Yen Postdoctoral fellowship from the Institute for Biophysical Dynamics at The University of Chicago and from an Arnold O. Beckman Postdoctoral Fellowship from the Arnold and Mabel Beckman Foundation. S.K. and S.-H.Y. were supported by Qatar National Research Fund exceptional Grant NPRPX-107-1-027. This work was completed in part with resources provided by the University of Chicago Research Computing Center. C.N.H and E.C.M. were supported by Grant BB/M000265/1 from the Biotechnology and Biological Sciences Research Council (U.K.) and an Advanced Award from the European Research Council (338895). Research in C.N.H.'s group was also supported by the Photosynthetic Antenna Research Center (PARC), an Energy Frontier Research Center funded by the U.S. Department of Energy, Office of Science, Office of Basic Energy Sciences under Award Number DE-SC 0001035. The authors thank Dr. Moira L. Flanagan for helpful discussions and Dr. Karen M. Watters for scientific editing.

■ REFERENCES

(1) Blankenship, R. E. *Molecular Mechanisms of Photosynthesis*, 2nd ed.; John Wiley & Sons, Ltd.: Chichester, West Sussex, 2014.

(2) Papiz, M. Z.; Prince, S. M.; Howard, T.; Cogdell, R. J.; Isaacs, N. W. The Structure and Thermal Motion of the B800−850 LH2 Complex from *Rps. acidophila* at 2.0Å Resolution and 100K: New Structural Features and Functionally Relevant Motions. *J. Mol. Biol.* **2003**, *326*, 1523−1538.

(3) Hess, S.; Akesson, E.; Cogdell, R. J.; Pullerits, T.; Sundstrom, V. Energy Transfer in Spectrally Inhomogeneous Light-Harvesting

DOI: 10.1021/acs.jpclett.8b03223
J. Phys. Chem. Lett. 2019, 10, 270−277

Pigment-Protein Complexes of Purple Bacteria. *Biophys. J.* **1995**, *69*, 2211−2225.
(4) Joo, T. H.; Jia, Y. W.; Yu, J. Y.; Jonas, D. M.; Fleming, G. R. Dynamics in Isolated Bacterial Light Harvesting Antenna (LH2) of *Rhodobacter sphaeroides* at Room Temperature. *J. Phys. Chem.* **1996**, *100*, 2399−2409.
(5) Hess, S.; Chachisvilis, M.; Timpmann, K.; Jones, M. R.; Fowler, G. J. S.; Hunter, C. N.; Sundstrom, V. Temporally and Spectrally Resolved Subpicosecond Energy Transfer Within the Peripheral Antenna Complex (LH2) and From LH2 To the Core Antenna Complex in Photosynthetic Purple Bacteria. *Proc. Natl. Acad. Sci. U. S. A.* **1995**, *92*, 12333−12337.
(6) Novoderezhkin, V.; Wendling, M.; van Grondelle, R. Intra- and Interband Transfers in the B800-B850 Antenna of *Rhodospirillum molischianum*: Redfield Theory Modeling of Polarized Pump-Probe Kinetics. *J. Phys. Chem. B* **2003**, *107*, 11534−11548.
(7) Cartron, M. L.; Olsen, J. D.; Sener, M.; Jackson, P. J.; Brindley, A. A.; Qian, P.; Dickman, M. J.; Leggett, G. J.; Schulten, K.; Hunter, C. N. Integration of Energy and Electron Transfer Processes in the Photosynthetic Membrane of *Rhodobacter sphaeroides*. *Biochim. Biophys. Acta, Bioenerg.* **2014**, *1837*, 1769−1780.
(8) Sener, M.; Strumpfer, J.; Singharoy, A.; Hunter, C. N.; Schulten, K. Overall Energy Conversion Efficiency of a Photosynthetic Vesicle. *eLife* **2016**, DOI: 10.7554/eLife.09541.
(9) Hess, S.; Feldchtein, F.; Babin, A.; Nurgaleev, I.; Pullerits, T.; Sergeev, A.; Sundstrom, V. Femtosecond Energy Transfer within the LH2 Peripheral Antenna of the Photosynthetic Purple Bacteria *Rhodobacter sphaeroides* and *Rhodopseudomonas palustris* LL. *Chem. Phys. Lett.* **1993**, *216*, 247−257.
(10) Kennis, J. T. M.; Streltsov, A. M.; Vulto, S. I. E.; Aartsma, T. J.; Nozawa, T.; Amesz, J. Femtosecond Dynamics in Isolated LH2 Complexes of Various Species of Purple Bacteria. *J. Phys. Chem. B* **1997**, *101*, 7827−7834.
(11) Fidler, A. F.; Singh, V. P.; Long, P. D.; Dahlberg, P. D.; Engel, G. S. Dynamic Localization of Electronic Excitation in Photosynthetic Complexes Revealed with Chiral Two-Dimensional Spectroscopy. *Nat. Commun.* **2014**, *5*, 3286−3291.
(12) Nagarajan, V.; Johnson, E. T.; Williams, J. C.; Parson, W. W. Femtosecond Pump-Probe Spectroscopy of the B850 Antenna Complex of *Rhodobacter sphaeroides* at Room Temperature. *J. Phys. Chem. B* **1999**, *103*, 2297−2309.
(13) Chachisvilis, M.; Kuhn, O.; Pullerits, T.; Sundstrom, V. Excitons in Photosynthetic Purple Bacteria: Wavelike Motion or Incoherent Hopping? *J. Phys. Chem. B* **1997**, *101*, 7275−7283.
(14) Pullerits, T.; Chachisvilis, M.; Sundstrom, V. Exciton Delocalization Length in the B850 Antenna of *Rhodobacter sphaeroides*. *J. Phys. Chem.* **1996**, *100*, 10787−10792.
(15) Book, L. D.; Ostafin, A. E.; Ponomarenko, N.; Norris, J. R.; Scherer, N. F. Exciton Delocalization and Initial Dephasing Dynamics of Purple Bacterial LH2. *J. Phys. Chem. B* **2000**, *104*, 8295−8307.
(16) Monshouwer, R.; Abrahamsson, M.; van Mourik, F.; van Grondelle, R. Superradiance and Exciton Delocalization in Bacterial Photosynthetic Light-Harvesting Systems. *J. Phys. Chem. B* **1997**, *101*, 7241−7248.
(17) Hybl, J. D.; Albrecht, A. W.; Gallagher Faeder, S. M.; Jonas, D. M. Two-Dimensional Electronic Spectroscopy. *Chem. Phys. Lett.* **1998**, *297*, 307−313.
(18) Cowan, M. L.; Ogilvie, J. P.; Miller, R. J. D. Two-Dimensional Spectroscopy Using Diffractive Optics Based Phased-locked Photon Echoes. *Chem. Phys. Lett.* **2004**, *386*, 184−189.
(19) Brixner, T.; Mancal, T.; Stiopkin, I. V.; Fleming, G. R. Phase-Stabilized Two-Dimensional Electronic Spectroscopy. *J. Chem. Phys.* **2004**, *121*, 4221−4236.
(20) Ramasesha, K.; Roberts, S. T.; Nicodemus, R. A.; Mandal, A.; Tokmakoff, A. Ultrafast 2D IR Anisotropy of Water Reveals Reorientation During Hydrogen-Bond Switching. *J. Chem. Phys.* **2011**, *135*, 054509.
(21) Ji, M.; Odelius, M.; Gaffney, K. J. Large Angular Jump Mechanism Observed for Hydrogen Bond Exchange in Aqueous Perchlorate Solution. *Science* **2010**, *328*, 1003−1005.
(22) Ji, M.; Gaffney, K. J. Orientational Relaxation Dynamics in Aqueous Ionic Solution: Polarization-Selective Two-Dimensional Infrared Study of Angular Jump-Exchange Dynamics in Aqueous 6M NaClO4. *J. Chem. Phys.* **2011**, *134*, 044516.
(23) Ni, Y.; Skinner, J. L. Ultrafast Pump-Probe and 2DIR Anisotropy and Temperature-Dependent Dynamics of Liquid Water Within the E3B Model. *J. Chem. Phys.* **2014**, *141*, 024509.
(24) Mehlenbacher, R. D.; Wang, J.; Kearns, N. M.; Shea, M. J.; Flach, J. T.; McDonough, T. J.; Wu, M. Y.; Arnold, M. S.; Zanni, M. T. Ultrafast Exciton Hopping Observed in Bare Semiconducting Carbon Nanotube Thin Films with Two-Dimensional White-Light Spectroscopy. *J. Phys. Chem. Lett.* **2016**, *7*, 2024−2031.
(25) Lewis, N. H.; Fleming, G. R. Two-Dimensional Electronic-Vibrational Spectroscopy of Chlorophyll *a* and *b*. *J. Phys. Chem. Lett.* **2016**, *7*, 831−837.
(26) Ostrander, J. S.; Knepper, R.; Tappan, A. S.; Kay, J. J.; Zanni, M. T.; Farrow, D. A. Energy Transfer Between Coherently Delocalized States in Thin Films of the Explosive Pentaerythritol Tetranitrate (PETN) Revealed by Two-Dimensional Infrared Spectroscopy. *J. Phys. Chem. B* **2017**, *121*, 1352−1361.
(27) Mehlenbacher, R. D.; McDonough, T. J.; Kearns, N. M.; Shea, M. J.; Joo, Y.; Gopalan, P.; Arnold, M. S.; Zanni, M. T. Polarization-Controlled Two-Dimensional White-Light Spectroscopy of Semiconducting Carbon Nanotube Thin Films. *J. Phys. Chem. C* **2016**, *120*, 17069−17080.
(28) Zanni, M. T.; Ge, N. H.; Kim, Y. S.; Hochstrasser, R. M. Two-Dimensional IR Spectroscopy Can be Designed to Eliminate the Diagonal Peaks and Expose Only the Crosspeaks Needed for Structure Determination. *Proc. Natl. Acad. Sci. U. S. A.* **2001**, *98*, 11265−11270.
(29) Read, E. L.; Engel, G. S.; Calhoun, T. R.; Mancal, T.; Ahn, T. K.; Blankenship, R. E.; Fleming, G. R. Cross-Peak-Specific Two-Dimensional Electronic Spectroscopy. *Proc. Natl. Acad. Sci. U. S. A.* **2007**, *104*, 14203−14208.
(30) Hamm, P.; Woutersen, S. Structure Determination of Trialanine in Water Using Polarization Sensitive Two-Dimensional Vibrational Spectroscopy. *J. Phys. Chem. B* **2000**, *104*, 11316−11320.
(31) Singh, V. P.; Westberg, M.; Wang, C.; Dahlberg, P. D.; Gellen, T.; Gardiner, A. T.; Cogdell, R. J.; Engel, G. S. Towards Quantification of Vibronic Coupling in Photosynthetic Antenna Complexes. *J. Chem. Phys.* **2015**, *142*, 212446.
(32) Harel, E.; Fidler, A. F.; Engel, G. S. Single-Shot Gradient-Assisted Photon Echo Electronic Spectroscopy. *J. Phys. Chem. A* **2011**, *115*, 3787−3796.
(33) Dahlberg, P. D.; Ting, P.-C.; Massey, S. C.; Allodi, M. A.; Martin, E. C.; Hunter, C. N.; Engel, G. S. Mapping the Ultrafast Flow of Harvested Solar Energy in Living Photosynthetic Cells. *Nat. Commun.* **2017**, *8*, 988−994.
(34) Fidler, A. F.; Singh, V. P.; Long, P. D.; Dahlberg, P. D.; Engel, G. S. Probing Energy Transfer Events in the Light Harvesting Complex 2 (LH2) of *Rhodobacter sphaeroides* with Two-Dimensional Spectroscopy. *J. Chem. Phys.* **2013**, *139*, 155101−155108.
(35) Ferretti, M.; Hendrikx, R.; Romero, E.; Southall, J.; Cogdell, R. J.; Novoderezhkin, V. I.; Scholes, G. D.; van Grondelle, R. Dark States in the Light-Harvesting Complex 2 Revealed by Two-Dimensional Electronic Spectroscopy. *Sci. Rep.* **2016**, *6*, 20834−20842.
(36) Walz, T.; Jamieson, S. J.; Bowers, C. M.; Bullough, P. A.; Hunter, C. N. Projection Structures of Three Photosynthetic Complexes from *Rhodobacter sphaeroides*: LH2 at 6 Å, LH1 and RC-LH1 at 25 Å. *J. Mol. Biol.* **1998**, *282*, 833−845.
(37) Georgakopoulou, S.; Frese, R. N.; Johnson, E.; Koolhaas, C.; Cogdell, R. J.; van Grondelle, R.; van der Zwan, G. Absorption and CD Spectroscopy and Modeling of Various LH2 Complexes from Purple Bacteria. *Biophys. J.* **2002**, *82*, 2184−2197.

DOI: 10.1021/acs.jpclett.8b03223
J. Phys. Chem. Lett. 2019, 10, 270−277

(38) Koepke, J.; Hu, X.; Muenke, C.; Schulten, K.; Michel, H. The Crystal Structure of the Light-harvesting Complex II (B800−850) from *Rhodospirillum molischianum*. *Structure* **1996**, *4*, 581−597.
(39) Ratsep, M.; Muru, R.; Freiberg, A. High Temperature Limit of Photosynthetic Excitons. *Nat. Commun.* **2018**, *9*, 99.
(40) Jimenez, R.; Dikshit, S. N.; Bradforth, S. E.; Fleming, G. R. Electronic Excitation Transfer in the LH2 Complex of *Rhodobacter sphaeroides*. *J. Phys. Chem.* **1996**, *100*, 6825−6834.
(41) Nagarajan, V.; Alden, R. G.; Williams, J. C.; Parson, W. W. Ultrafast Exciton Relaxation in the B850 Antenna Complex of *Rhodobacter sphaeroides*. *Proc. Natl. Acad. Sci. U. S. A.* **1996**, *93*, 13774−13779.
(42) Lakowicz, J. R. *Principles of Fluorescence Anisotropy*, 3rd ed.; Springer: New York, 2006.
(43) Wynne, K.; Hochstrasser, R. M. Coherence Effects in the Anisotropy of Optical Experiments. *Chem. Phys.* **1993**, *171*, 179−188.
(44) Wang, Y.-P.; Du, L.-C.; Zhu, G.-B.; Wang, Z.; Weng, Y.-X. Synchronous Measurement of Ultrafast Anisotropy Decay of the B850 in Bacterial LH2 Complex. *Chin. Phys. Lett.* **2015**, *32*, 023101.
(45) Segatta, F.; Cupellini, L.; Jurinovich, S.; Mukamel, S.; Dapor, M.; Taioli, S.; Garavelli, M.; Mennucci, B. A Quantum Chemical Interpretation of Two-Dimensional Electronic Spectroscopy of Light-Harvesting Complexes. *J. Am. Chem. Soc.* **2017**, *139*, 7558−7567.
(46) Sohail, S. H.; Dahlberg, P. D.; Allodi, M. A.; Massey, S. C.; Ting, P.-C.; Martin, E. C.; Hunter, C. N.; Engel, G. S. Communication: Broad Manifold of Excitonic States in Light-harvesting Complex 1 Promotes Efficient Unidirectional Energy Transfer *in vivo*. *J. Chem. Phys.* **2017**, *147*, 131101.

DOI: 10.1021/acs.jpclett.8b03223
J. Phys. Chem. Lett. 2019, 10, 270−277